DYNAMICALLY GATED MIXTURE OF EXPERTS FOR MULTI-TASK REINFORCEMENT LEARNING

Anonymous authors
Paper under double-blind review

ABSTRACT

Multi-task reinforcement learning (MTRL) promises unique strengths against single-task RL because of generalization across tasks through parameter sharing and composition. Existing methods rely on local routing or static compositional weights in Mixture-of-Experts (MoE) without the ability to adapt to evolving temporal context. To improve the inherently temporal and dynamic systems in MTRL, we introduce a global recurrent inhibition network (GRIN) that performs dynamic gating across time, selectively modulating expert activations based on temporally accumulated context. Our formulation propagates information across time steps to preserve global activation information across the model. Notably, using the gating approach, we found statistically significant improvements over state-of-the-art MTRL methods, with an empirical **+3.7%** improvement on the Metaworld MT50 benchmark.

1 INTRODUCTION

Deep reinforcement learning has demonstrated the capacity to acquire complex behaviors across diverse domains Mnih et al. (2013); Gu et al. (2017); Kalashnikov et al. (2018); Lillicrap et al. (2015). The human ability to leverage similar tasks to learn to perform many tasks inspires multi-task reinforcement learning (MTRL), which offers a path toward more general agents. To enable sharing of knowledge and parameters, Mixture-of-experts and compositional parameter-sharing approaches Hendawy et al. (2023); Sun et al. (2022) have shown promise by enabling task-specific specialization within unified architectures. However, these methods typically rely on local routing or static compositional weights, limiting adaptability as temporal context evolves during an episode.

Gating mechanisms have proven effective for controlling information flow in neural networks, such as LSTMs Hochreiter & Schmidhuber (1997) and notably, to modern attention and LLM architectures Qiu et al. (2025). Recent work Qiu et al. (2025) demonstrates that dynamic, input-dependent gating applied across time enhances nonlinear expressivity and improves optimization stability. We investigate whether these benefits extend to the complex temporal dynamics of MTRL, where agents must continuously adapt behavior based on evolving task demands. We introduce a global recurrent inhibition network (GRIN) that performs dynamic gating across time steps, selectively modulating feature activations based on temporally accumulated context.

A key challenge in applying gating to model-free deep RL is that feedforward networks restrict gating inputs to preceding layers within the current forward pass, forfeiting access to global information. Our formulation addresses this by propagating activations forward across time steps, enabling the gate to leverage any activation from the previous step and preserve global context. This mechanism directly parallels cortical inhibitory neurons that integrate diverse synaptic inputs to orchestrate neural computation.

We show that in multi-task settings, global network gating with input access to Q-value and task-specific signals enhances model performance. GIN achieves 90.0% on the Metaworld MT10 benchmark, and demonstrates a statistically significant **+3.7%** improvements with our reproduced results on the challenging MT50 benchmark. These results demonstrate that temporal gating yields improvements over state-of-the-art MTRL methods, establishing dynamic gating across time as an effective mechanism for multi-task policy learning.

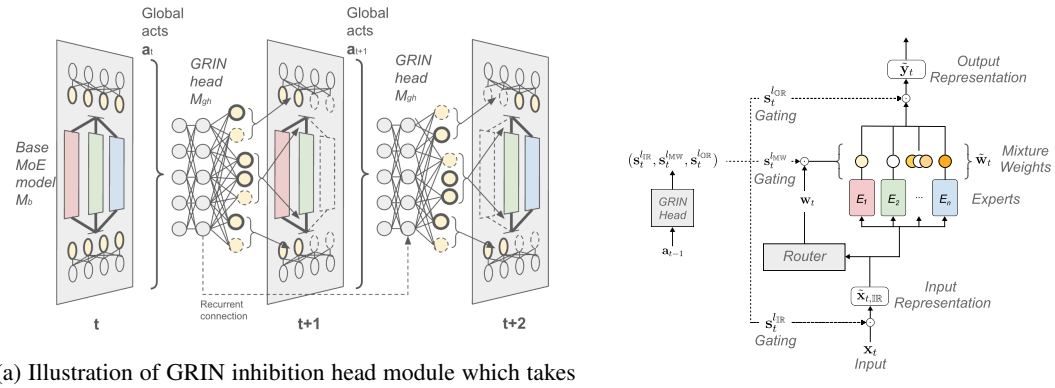

(a) Illustration of GRIN inhibition head module which takes in all global activations and dynamically changes the MoE weights and architecture.

(b) MoE preliminaries and GRIN gating locations.

Figure 1: Model Architecture

2 Background and Related Work

A rich body of work in MTRL has explored diverse strategies for achieving effective generalization across tasks. The paper D'Eramo et al. (2024) established theoretical foundations showing that MTRL yields increasing benefits as the number of tasks grows, whileTeh et al. (2017) propose learning individual task policies that share a common prior. The Meta-World benchmark Yu et al. (2020b) has become a standard testbed for robotic manipulation, typically trained with Soft Actor-Critic Haarnoja et al. (2018). However, naive parameter sharing can induce negative transfer when task gradients conflict. The paper Yu et al. (2020a) address this through gradient projection methods that orthogonalize task gradients, though such approaches can be sensitive to gradient variance. Modular architectures offer an alternative: Yang et al. (2020) introduce routing networks that generate task-specific parameters from a shared base model, and Devin et al. (2017) decompose policy responsibilities across robot-specific and task-specific modules. More recent work conditions shared representations on task context: Sodhani et al. (2021) learn a mixture of state encoders using task metadata, producing diverse and interpretable representations, while Perez et al. (2018) leverages feature-wise linear modulation for task conditioning.

Deep learning has designed adaptation and inhibitive mechanisms through learnable gating architectures that selectively amplify or suppress features. These appear in LSTMs (Hochreiter & Schmidhuber, 1997), Highway Networks (Srivastava et al., 2015), and Gated Linear Units (GLUs) (Dauphin et al., 2017b; Shazeer, 2020), where they prevent gradient vanishing, and enhance network sparsity. The mechanism mirrors biological cortical inhibition, where diverse inhibitory neurons modulate excitatory activity to maintain network stability and sharpen signal selectivity (Isaacson & Scanziani, 2011; Klausberger & Somogyi, 2008; Tremblay et al., 2016). Studies reveal remarkable diversity in inhibitory connectivity patterns inhibition(Gidon & Segev, 2012; Markram et al., 2004; Chini et al., 2022).

Dropout and its variants (Ba & Frey, 2013; Kingma et al., 2015; Ghiasi et al., 2018; Liu et al., 2022; Zhao et al., 2022; Li et al., 2023) demonstrate the effectiveness of stochastic adaptation during training. Capsules (Hinton et al., 2011; Sabour et al., 2017; Hinton et al., 2018) leverage dynamic routing at the unit and layer level, and remains an area of novel active research. In comparison, we focus on a global approach to improve existing ML models and MoE.

Different from prior work, we propose a global approach across the model. The propagation across time builds a global, dynamic adaptation module. This module aggregates signals from any part of the neural network and modulate MoE pathways. This design enables GRIN to provide a general mechanism for dynamic modulation. We demonstrate its effectiveness in multi-task reinforcement learning, as well as in computer vision and limited-scale language models.

3 ALGORITHM AND METHODS

3.1 PRELIMINARIES

Mixture of Experts (MoE) (Shazeer et al., 2017) architectures dynamically route inputs through specialized sub-networks. A standard MoE layer transforms an input representation ($\mathbb{IR}$) $\mathbf{x}_{\mathbb{IR}} \in \mathbb{R}^d$. In an MoE without a router model (Sun et al., 2022), $\mathbf{x}_{\mathbb{IR}}$ is transformed by the experts then aggregated by mixture weights ($\mathbb{MW}$) which could be either fixed or learned. In a gated MoE, $\mathbf{x}_{\mathbb{IR}}$ is put to a router model that computes mixture weights $\mathbf{w}_{\mathbb{MW}} = \text{Router}(\mathbf{x}_{\mathbb{IR}})$, and $\mathbf{w}_{\mathbb{MW}} = [w_1, w_2, ...]$ where w_i represents the contribution of the i-th expert out of N experts. After $\mathbf{x}_{\mathbb{IR}}$ is propagated through the expert models, an aggregation step combines expert outputs. The final output representation ($\mathbb{OR}$) is computed as: $\mathbf{y}_{\mathbb{OR}} = \sum_{i=1}^{N} w_i \cdot E_i(\mathbf{x}_{\mathbb{IR}})$, where E_i denotes the i-th expert network and N is the total number of experts. Variants include mixed MoE where all experts process inputs with soft weights from a softmax router, gated MoE that adds learnable gates to modulate expert contributions, and sparsely-gated MoE that selects only the top-k experts for efficiency.

To enable precise control over network modulation, we design the GRIN head module to dynamically regulate MoE architectures. Generic MoE leverages three key representations: the input representation ($\mathbb{IR}$), the mixture weights ($\mathbb{MW}$), and the output representation ($\mathbb{OR}$). The GRIN head module generates gating masks through sigmoid non-linearity (Dauphin et al., 2017a), directly modulating these representations.

3.2 GRIN ARCHITECTURE WITH THE HEAD MODULE

The limitation of existing MoE approaches is that gating decisions are made locally based solely on the current input representation $\mathbf{x}_{\mathbb{IR}}$, without considering global network activation patterns or interactions between experts. We propose Global Recurrent Inhibition Networks (GRIN) that modulate the MoE architecture at three critical locations[1]—input representations ($\mathbb{IR}$), mixture weights ($\mathbb{MW}$), and output representations ($\mathbb{OR}$)—using inhibition masks ($\mathbf{s}$) derived from global network activations:

$$\tilde{\mathbf{a}}^l = \mathbf{s}^l \odot \mathbf{a}^l, \quad \text{for } l \in \{l_{\mathbb{IR}}, l_{\mathbb{MW}}, l_{\mathbb{OR}}\} \quad \text{where } \mathbf{s}^{l_{\mathbb{IR}}}, \mathbf{s}^{l_{\mathbb{MW}}}, \mathbf{s}^{l_{\mathbb{OR}}} = \sigma(\mathcal{G}(\mathbf{a}_{global})). \tag{1}$$

Here $\mathbf{a}^l$ denotes the original activation at location l, $\mathbf{s}^l$ denotes the inhibition mask computed by the GRIN head $\mathcal{G}$ from global activations $\mathbf{a}_{global}$ with the ending sigmoid non-linearity σ, $\odot$ denotes element-wise multiplication, and $\tilde{\mathbf{a}}^l$ denotes the gated activation. This formulation enables dynamic, globally-aware modulation that considers the full network state when making modulation and gating decisions.

As shown in Figure 1a and Figure 1b, the GRIN head model operates as a modulator and controller, taking in the global activations and producing the inhibition masks. The inhibition masks are applied to elements of the MoE model, on mixture weights ($l_{\mathbb{MW}}$) of the MoE model, which determines the weighting or selection of each expert. The other category of gating for the GRIN head is to modulate and modify the input representation ($l_{\mathbb{IR}}$) as well as the output representation ($l_{\mathbb{OR}}$) of the MoE model.

For a base model with MoE architecture, GRIN is defined as $\Gamma = (\mathcal{X}, \mathcal{M}, \mathcal{G}, \mathcal{A}, \mathcal{S}, \mathcal{L})$, where $\mathcal{X}$ denotes input data, $\mathcal{M}$ is the base MoE model, $\mathcal{G}$ is the GRIN head, $\mathcal{A}$ represents base model activations, $\mathcal{S}$ are the inhibition masks (gating masks), and $\mathcal{L}$ specifies gating target locations, and $\mathcal{L} = \{l_{\mathbb{IR}}, l_{\mathbb{MW}}, l_{\mathbb{OR}}\}$. The system evolves through discrete time steps with state representations $\mathcal{D} = \{(\mathbf{x}_t, \mathbf{a}_t, \mathbf{h}_t, \mathbf{s}_t)\}$, where $\mathbf{x}_t \in \mathbb{R}^n$, $\mathbf{a}_t \in \mathbb{R}^m$, $\mathbf{h}_t \in \mathbb{R}^k$, and $\mathbf{s}_t \in \mathbb{R}^p$.

[1] We define a location to be one or more layers, units or connections in the network.

Algorithm 1 GRIN Forward Pass

Require: Input $\mathbf{x}_t$, Number of recurrent steps T, GRIN head $\mathcal{G}$, base model $\mathcal{M}$

for $iter = 1$ to N **do**
  Initialize $\mathbf{s}_0 \leftarrow \mathbf{1}$, $\mathbf{h}_0$, $\mathbf{h}_{-1}$
  for $t = 1$ to T **do**
    $\mathbf{h}_{t-1} \leftarrow f_{\text{RNN}}(\mathbf{h}_{t-2}, \tilde{\mathbf{a}}_{t-1})$ ▷ Update hidden state
    $\mathbf{s}_t^{l_{\text{IR}}}, \mathbf{s}_t^{l_{\text{MW}}}, \mathbf{s}_t^{l_{\text{OR}}} \leftarrow \sigma(\mathbf{W}_{\text{GRIN}}\mathbf{h}_{t-1} + \mathbf{b}) = \sigma(\mathcal{G}(\mathbf{h}_{t-2}, \tilde{\mathbf{a}}_{t-1}))$
    $\mathbf{a}_t^{l_{\text{IR}}}, \mathbf{a}_t^{\text{pretext}} \leftarrow \mathcal{M}_{\text{Pretext}}(\mathbf{x}_t)$ ▷ Forward pretext model
    $\tilde{\mathbf{a}}_t^{l_{\text{IR}}} \leftarrow \mathbf{s}_t^{l_{\text{IR}}} \odot \mathbf{a}_t^{l_{\text{IR}}}$ ▷ Modulate input repres.
    $\mathbf{w}_t \leftarrow \text{Router}(\tilde{\mathbf{a}}_t^{l_{\text{IR}}})$ ▷ Compute mixture weights
    $\tilde{\mathbf{w}}_t \leftarrow \mathbf{s}_t^{l_{\text{MW}}} \odot \mathbf{w}_t$ ▷ Modulate mixture weights
    $\mathbf{a}_t^{l_{\text{OR}}} \leftarrow \sum_{i=1}^{N} \tilde{w}_{i,t} \cdot E_i(\tilde{\mathbf{a}}_t^{l_{\text{IR}}})$ ▷ Aggregate outputs
    $\tilde{\mathbf{a}}_t^{l_{\text{OR}}} \leftarrow \mathbf{s}_t^{l_{\text{OR}}} \odot \mathbf{a}_t^{l_{\text{OR}}}$ ▷ Modulate output
    $\mathbf{a}_t^{\text{post}} \leftarrow \mathcal{M}_{\text{post}}(\tilde{\mathbf{a}}_t^{l_{\text{OR}}})$ ▷ Forward post model
    $\tilde{\mathbf{a}}_t \leftarrow \{\mathbf{a}_t^{\text{pretext}}, \tilde{\mathbf{a}}_t^{l_{\text{IR}}}, \tilde{\mathbf{a}}_t^{l_{\text{OR}}}, \mathbf{a}_t^{\text{post}}\}$ ▷ Aggregate activations
    Compute $\mathbf{loss}_t$
    BackProp $\mathbf{loss}_t$
    $\theta \leftarrow \theta + \Delta\theta$
  end for
end for

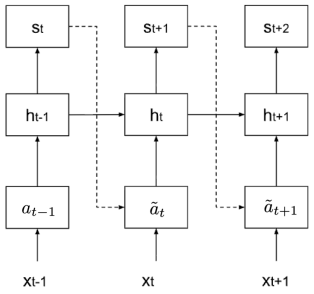

Figure 2: Recurrent network for GRIN with respect to activations, hidden states, and inhibition masks.

3.3 GRIN Recurrent Formulation

GRIN employs a recurrent formulation where the inhibition masks are iteratively refined over T time steps, allowing the network to observe and respond to its own activation patterns. As shown in Figure 2, at each timestep t, the GRIN head processes the current gated activations $\tilde{\mathbf{a}}_t$, the hidden state $\mathbf{h}_t$, and the previous hidden state $\mathbf{h}_{t-1}$ to compute updated inhibition masks $\mathbf{s}_{t+1}$, which modulate the network's forward pass. This recurrent mechanism enables the network to iteratively refine the modulation of expert weights and representations by incorporating feedback from previous choices. The state evolution is governed by the following dynamics:

$$\begin{aligned} \mathbf{h}_t &= f_{\text{RNN}}(\mathbf{h}_{t-1}, \tilde{\mathbf{a}}_t) \\ \mathbf{s}_{t+1} &= \sigma(\mathbf{W}_{\text{GRIN}} \cdot \mathbf{h}_t + \mathbf{b}) = \sigma(\mathcal{G}(\mathbf{h}_{t-1}, \tilde{\mathbf{a}}_t)) \\ \tilde{\mathbf{a}}_{t+1}^{l_{\text{OR}}} &= \mathcal{M}_{\text{MoE}}(\mathbf{x}_{\text{IR}} \odot \mathbf{s}_t^{l_{\text{IR}}}, \mathbf{w}_{\text{MW}} \odot \mathbf{s}_t^{l_{\text{MW}}}) \odot \mathbf{s}_t^{l_{\text{OR}}} \end{aligned} \tag{2}$$

where f_{RNN} can be any recurrent cell (LSTM, GRU), $\mathbf{s}_t = \{\mathbf{s}_t^{l_{\text{IR}}}, \mathbf{s}_t^{l_{\text{MW}}}, \mathbf{s}_t^{l_{\text{OR}}}\}$ are the inhibition masks at timestep t, and $\mathcal{M}_{\text{MoE}}(\cdot)$ denotes the modulated MoE forward pass using inhibition masks $\mathbf{s}_t$. During training, gradients flow through all timesteps via backpropagation through time, jointly optimizing the base model and GRIN head. Algorithm 1 presents the full GRIN recurrent algorithm.

3.4 Training, Optimization, and Inference

During training and across recurrence steps, the gradient computation graph is kept and we perform gradient back-propagation across time to optimize the recurrent neural network. We note that in the case of GRIN, when the data input is non-sequential, we choose to use the same $\mathbf{x}$ to propagate multiple time-steps. This simulates the dynamic changes in the base-model with the same data input, but across different time steps. When we use GRIN to recurrently forward propagate T steps, it is a choice to back-propagate at each time step, and sum the gradients over time. This offers a higher quality gradient for the optimization. At inference time, the pretex inhibition and GRIN models can operate on the data points sampled from the test set.

4 Experiments on multi-task Reinforcement Learning

We evaluate the GRIN algorithm on the MetaWorld benchmark with the multi-task reinforcement learning (MTRL). MetaWorld offers a suite of reinforcement learning environments comprising up to 50 robotic manipulation tasks. In our RL model, both the actor and critic networks employ Mixture-of-Experts (MoE) architectures with orthogonalization, while the mixture-weight encoder is conditioned solely on the task-ID.

Table 1: MT10 Average Success Rate (%): comparison of GRIN with prior methods

Method	Epoch 1 % (1M)	Epoch 2 % (2M)	Epoch 3 % (3M)	Epoch 5 % (5M)	Epoch 10 % (10M)	Epoch 15 % (15M)	Epoch 20 % (20M)
SAC (Yu et al., 2019)	10.0±8.2	17.7±2.1	18.7±1.1	20.0±2.0	48.0±9.5	57.7±3.1	61.9±3.3
MTSAC (Yu et al., 2019)	34.9±12.9	49.3±9.0	57.1±9.8	60.2±9.6	61.6±6.7	65.6±10.4	62.9±8.0
SAC+FiLM (Perez et al., 2017)	32.7±6.5	46.9±9.4	52.9±6.4	57.2±4.2	59.7±4.6	61.7±5.4	58.3±4.3
PCGrad (Yu et al., 2020)	32.2±6.8	46.6±9.3	54.0±8.4	60.2±9.7	62.6±11.0	62.6±10.5	61.7±10.9
Soft-Module (Yang et al., 2020)	24.2±4.8	41.0±2.9	47.4±5.3	51.4±6.8	53.6±4.9	56.6±4.8	63.0±4.2
CARE (Sodhani et al., 2021)	26.0±9.1	52.6±9.3	63.8±7.9	66.5±8.3	69.8±5.1	72.2±7.1	76.0±6.9
PaCo (Sun et al., 2022)	30.5±9.5	49.8±8.2	65.7±4.5	64.7±4.2	71.0±5.5	81.0±5.9	85.4±4.5
MOORE (Hendawy et al., 2024)	36.4±7.8	64.4±5.5	72.1±6.5	74.8±4.0	80.1±6.1	84.8±4.3	88.4±3.4
MOORE (**IQM**±std)	33.5±4.3	65.0±4.0	72.8±4.0	74.2±3.3	79.8±0.4	84.8±4.3	89.5±0.3
GRIN (Ours)	**45.7**±9.1	63.7±3.0	68.3±5.3	**78.4**±5.8	**83.0**±4.4	**87.7**±3.5	**89.4**±1.0
GRIN (Ours, **IQM**±std)	**45.4**±5.0	63.3±0.4	69.0±1.7	**78.3**±0.4	**81.5**±2.6	89.4±0.9	**90.0**±0.0[4]

Aligned with the experiment procedures of the previous work, we use the soft-actor-critic (SAC) model with a 3-layer fully connected neural network each with 400 hidden units and *tanh* non-linearity. We use 4 experts MoE model for the MT10 experiment and 6 experts MoE for the MT50 experiment. The multi-head architecture is used after the MoE. Our experiments are performed with GRIN gating on both $l_{\mathbb{MW}}$, and $l_{\mathbb{OR}}$ locations, and implemented in the MoE algorithm with task-encoder (Sun et al., 2022) and orthogonalization (Hendawy et al., 2023). The MoE architecture and GRIN are used for both Actor and Critic networks, but GRIN does not have connections across the two network. In each epoch we run the soft-actor-critic algorithm with GRIN for 100,000 iterations, with batch size of 128. For evaluation, we follow Agarwal et al. (2021) to compute the interquartile mean (IQM) of success rates across random seeds for both MT10 and MT50. Robust to outlier scores, the IQM computes the mean on the middle 50% of combined runs, after ranking the random seeds with their success rates. For the standard deviation calculation in the IQM column of the tables, the bottom and top 25% of the data are excluded. For both MT10 and MT50 comparison against MOORE Hendawy et al. (2023), we report the success rate metrics obtained by *reproducing* the authors results by running their open-source code.[2].

4.1 GRIN shows best IQM results MetaWorld MT10

In Table 1, we report the evaluation success rates for MT10 in the MetaWorld environment. The mean and standard deviation of the success rate are computed across 10 random seeds. The GRIN algorithm consistently improves upon the MoE-based MTRL algorithm, despite the performance plateauing effect in MT10 also reported in (Hendawy et al., 2023). In Table 1, we also compare selected epochs with prior algorithms, including the recent PaCo (Sun et al., 2022) and MOORE approaches (Hendawy et al., 2023). We further note the MT10 success rate of 0.8923 ± 0.0112 reported in the recent work (Kong et al., 2025). GRIN (ours) surpasses this result, while we note that (Kong et al., 2025) reported using only 3 random seeds [3].

4.2 GRIN shows significant improvement over prior art on MetaWorld MT50

We evaluate GRIN on the MetaWorld MT50 benchmark (MT50) with 50 distinct tasks. Our implementation builds upon the orthogonalized mixture-of-experts (MOORE) framework proposed by Hendawy et al. (Hendawy et al., 2023), employing six experts for both actor and critic networks with global activation intake and a recurrence depth of 1, as determined optimal in our ablation studies.

Table 2 presents the success rates and the IQM results comparing GRIN against MOORE, the current state-of-the-art method. Our results demonstrate that GRIN achieves substantial improvements over MOORE, with notable performance gains at 50M, 100M, and 175M environment steps. These results suggest that the global gating and modulation mechanism in GRIN effectively enhances the model's ability to handle the diverse task distribution in MT50. We note that although our reproduction results with open-source code didn't reach the reported numbers in Hendawy et al. (2023), the statistically significant improvement are clearly shown in the results. GRIN algorithm improved IQM results by **+3.7%** at 100M env. steps, shown in Table 2. This improvement sustains even as we continue to run the algorithms to 175M env. steps, as shown in Table 3.

[2]We used: https://github.com/AhmedMagdyHendawy/MOORE.

[3]Appendix B5 of (Kong et al., 2025)

[4]The success rate data for random seeds excluding bottom 25% and top 25% are all 90%.

Algorithm	Env. st.	Ave. suc.	**IQM**
MTSAC (Yu+ 19)	100M	49.3±1.5%	–
SAC+FiLM (Perez+ 17)	100M	36.5±12.0%	–
CARE (Sodhani+ 21)	100M	50.8±1.0%	–
PaCo (Sun+ 22)	100M	57.3±1.3%	–
MOORE (Our repro.)	50M	51.2±2.1%	–
GRIN (Ours)	50M	**55.7**±2.9%	–
MOORE (Our repro.)	100M	55.7±2.8%	56.1±0.9%
GRIN (Ours)	100M	**59.9**±1.6%	**59.8**±0.2%

Table 2: Metaworld MT50 results.

Algorithm	Env. st.	**IQM**
MOORE (Our repro.)	175M	62.1±0.5%
GRIN (Ours)	175M	**63.4**±1.0%
GRIN (Ours)	250M	**64.4**±1.0%

Table 3: Extended run on MT50.

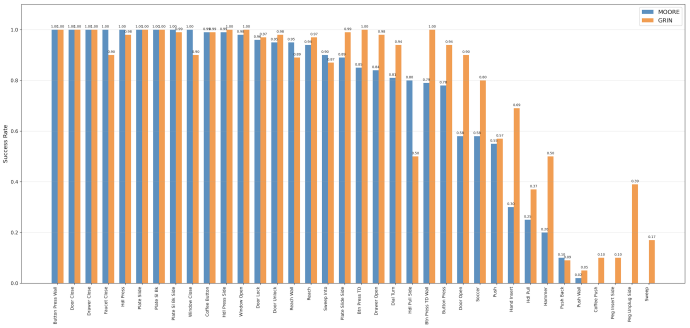

Figure 3: MT50 tasks success rate comparison GRIN compared with MOORE, reported at 50M env. steps.[5]

In Figure 3, we show the per-task performance of GRIN compared with the prior MOORE algorithm. Several tasks exhibit significant improvements. Out of 36 tasks with non-zero success rates, GRIN achieves higher success rates than MOORE on 22 tasks (61%). In contrast, MOORE outperforms GRIN on 8 tasks (17%).

4.3 Analysis with Off Policy Evaluation

In the MetaWorld MT10 environment, we perform off-policy evaluation by collecting 150,000 transitions in offline trajectories across tasks.

For each transition, Q values for GRIN, and MOORE as baseline, are computed with $Q = F_{\text{critic}}(s_t, a_t^*)$ where s_t is the transition state, and $a_t^* = F_{\text{actor}}(s_t)$. During the forward compute, we collected the output representation ($\mathbb{OR}$) inhibition masks, the mixture weight ($\mathbb{MW}$) inhibition masks, which are used to compute average inhibition levels. Table 4 shows $\mathbb{OR}$ inhibition levels correlates the most with the Q value. In comparison the inhibition levels on mixture weights are less significant. This finding indicates GRIN's modulation may play a larger role compared to routing data in MTRL. Across data in all transitions, we fit Gaussian distributions to the baseline model's and GRIN's Q values for a Fitted Q Evaluation (FQE) analysis. Figure 4 shows the Q value improvement with GRIN is on average 8.5, and 93.5% of the samples observed improvement in Q with GRIN. Finally, we present a segment analysis. The data is segmented by the median in actor inhibition level[6]. On the top of Figure 5 we show histogram plot of Q values of transitions with more actor $\mathbb{OR}$ inhibition (above median), and on the bottom we show the plot for transitions with less. With more inhibition, we observe more improvement (+10.2) across the median of GRIN Q values vs baseline. This value is smaller (+9.5) in the opposing segment. The value distributions are visibly different across more vs less inhibition. The result shows the effectiveness and significance of modulation from the GRIN head model.

4.4 Ablation Studies

[6]We compute the average across the hidden units for Actor $\mathbb{OR}$ inhibition masks, and find the median across the transitions. The median value is 0.105.

Table 4: Inh. corr. & Q improvements

Metric	Value	Desc.
$\mathbb{OR}$ *Inhibition*	*Corr.*	
Actor → GRIN Q	$+0.47$	+ve
Actor → Q impr.	$+0.31$	+ve
Critic → GRIN Q	$+0.19$	Weak +ve
Critic → Q impr.	$+0.14$	Weak +ve
$\mathbb{MW}$ *Inhibition*	*Corr.*	
Actor → Q	-0.08	Slight -ve
Critic → Q	–	Negligible
Q-Value Performance		
Improved samples	93.5%	–
Mean impr.	8.5 ± 7.0	–

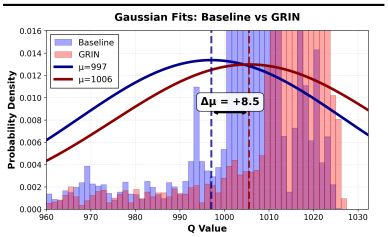

Figure 4: FQE Gaussian fit of GRIN Q values vs Baseline.

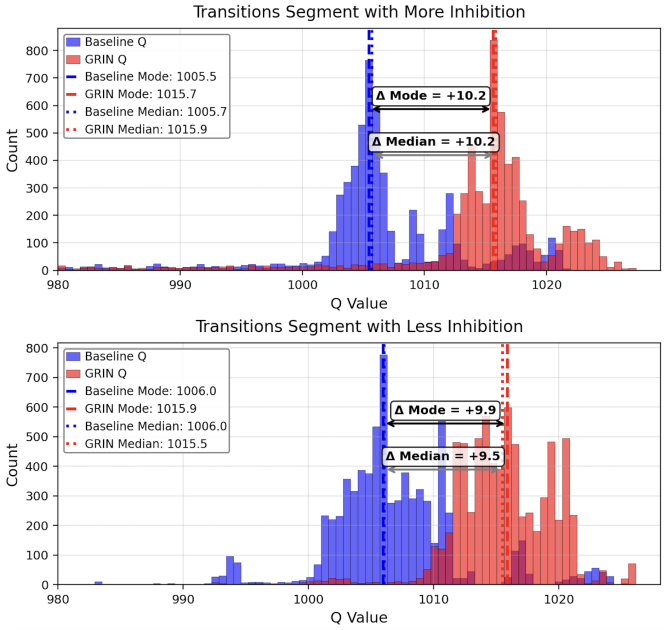

Figure 5: Segment Analysis for transitions with More $\mathbb{OR}$ inhibition (inhibition mask mean level is below the data median *0.105*) vs Less.

Recurrent depth. We conduct ablation studies on the Meta-World MT5 benchmark comprising five tasks to evaluate GRIN with recurrence depths ranging from 1 to 3. The recurrent implementation follows Algorithm 1. As shown in Table 5 and Figure6, a recurrence depth of 1 yields optimal success rates indicating a single recurrence step is typically sufficient for less complex MTRL tasks. **Number of experts**. We evaluate GRIN's effectiveness by varying expert capacities across 3, 4, and 6 experts, keeping other parameters constant. Results in Figure 6 show that for the MT5 task, expanding the expert pool didn't significantly improve the results. We also perform the experiment on Minigrid Chevalier-Boisvert et al. (2023) MT7[7] shown in Table 6 and observe similar results. Although increasing the number of experts offered less improvements, the ablation aligns with results with the MT10 Q-value correlation in Table 4, and verifies that GRIN contributes more through modulation on the representations.

Setting	Succ. rate (%)
Number of Recursion Steps	
1 step (baseline)	91.3 ± 8.4
2 steps	76.7 ± 2.5
3 steps	78.0 ± 2.8
Number of Experts	
3 Experts (baseline)	91.3 ± 8.4
4 Experts	78.7 ± 0.9
6 Experts	82.0 ± 4.3
Modulation and Gating Location	
$\mathbb{OR} + \mathbb{MW}$ (baseline)	91.3 ± 8.4
$\mathbb{OR}$ only	90.7 ± 7.7
$\mathbb{MW}$ only	80.7 ± 5.2

Table 5: MT5 Ablation with GRIN

Selectivity from global inputs. Global activations make the inhibition head effective for modulation the network. While since there is a variety of base model architectures, the selection of inputs may be needed. We offer an ablation using Minigrid, which uses a convolutional net. In the base GRIN setting, we connect the 2-D structured pretext layers to the inhibition head, while in GRIN light, we only connect the post model and the MoE output to the inhibition head. Interestingly, the light version performs well. So it may be effective to perform input selection from a global set of network activations.

Gating mask location $\mathcal{L}$. We investigate the optimal point of intervention for GRIN's inhibition signal by applying the gating mask at three distinct locations in the MoE architecture: (a) the mixture weights that determine expert contributions ($l^{\mathbb{MW}}$), and (b) the combined output representation after expert aggre-

Algorithm	4 Experts	6 Experts	8 Experts
MOORE	74.4 ± 7.1	71.5 ± 9.3	78.1 ± 3.9
GRIN	73.1 ± 5.2	78.3 ± 6.5	73.4 ± 8.3
GRIN light	76.3 ± 5.4	76.7 ± 7.6	76.6 ± 5.4

Table 6: Minigrid MT7 succ. rate (%)

[7]Experiments were run with 10 random seeds across 50 epochs.

gation ($l^{\mathbb{OR}}$). We observe the inhibition mechanism is most effective at the output representation ($l^{\mathbb{OR}}$) by selectively suppressing patterns in the aggregated output. The result aligns with the correlations in Table 4, and is helpful to inform optimal architectural integration of recurrent inhibition mechanisms.

5 GENERALIZING TO ML DOMAINS

The primary application of GRIN on MTRL shows its capability for state-space models. We make efforts to generalize GRIN to other ML domains. To ensure it is efficient to grow GRIN's parameter size, we explore a cascade of progressively increasing input diversity.

5.1 CASCADING INPUT DIVERSITY

Inhibitory neurons constitute a small portion of the neural population (Swanson & Maffei, 2019), and they exhibit remarkable diversity (Hofer et al., 2011; Pfeffer et al., 2013; Kajiwara et al., 2021). We focus on the diversity of input connections to translate this connection diversity to the GRIN head module ($\mathcal{G}$):

Pretext Inhibition (PRE): The gating mechanism operates on incomplete forward-pass information, using the activations available up to the current layer (the pretext). Gated Linear Unit (GLU) is a special instance.

Cross-iteration Global Inhibition (CIGI): We processes all activations from the previous stochastic optimization batch through a dedicated inhibition head to generate gating masks. Pooling operations are applied across the batch, producing sample-agnostic inhibition masks to gate the activations of the current iteration.

Global Recurrent Inhibition Network (GRIN): GRIN algorithm was described in Section 3 which not only can produce specific masks per data sample, but also refine the adaptive gating decisions iteratively.

The inhibition head model combines information from multiple sources to compute the inhibition masks:

$$\mathbf{s}_{t+1} = \sigma(\mathcal{G}(\mathbf{a}_{global})) = \sigma(\mathbb{I}_{\text{PRE}} W_{\text{PRE}} \cdot f_{\text{PRE}}(\mathbf{a}_t) + \mathbb{I}_{\text{CIGI}} W_{\text{CIGI}} \cdot f_{\text{CIGI}}(\mathbf{a}^*_{t-1}) + \mathbb{I}_{\text{GRIN}} W_{\text{GRIN}} \cdot \mathbf{h}_t + b) \tag{3}$$

where $\mathbb{I}$ are indicator functions to select the existence of the connection; $\mathbf{a}^*_{t-1}$ represents pooled activations from the previous batch in CIGI. At training time for CIGI, the inhibition head and base model are jointly optimized. At inference time, when evaluating a new data point, we sample a batch of test data to simulate its prior iteration, producing the pooled inhibition masks.

5.2 HAND-WRITTEN DIGITS AND NUMBER OF SQUARES

To generalize to the vision domain, we built a bi-modal simulated dataset comprising 120,000 samples, composed of half MNIST handwritten digits and half synthetic number patterns(Stoianov & Zorzi, 2012). Each sample is labeled with its numeric value (0-9). We use a convnet with a sparsely gated MoE with fully connected layers(Shazeer et al., 2017).

Algorithm	Acc.	Std.
Baseline model	81.4%	1.7e-2
MoE 3/5 experts	92.3%	5.6e-2
Random (dropout 0.25)	94.9%	2.0e-2
Random (dropout 0.5)	95.1%	1.9e-2
Random (dropout 0.75)	95.9%	8.1e-3
One-layer I. (GLU)	95.2%	5.1e-3
PRE	95.3%	8.4e-3
CIGI	94.9%	2.3e-3
GRIN	**96.3%**	1.0e-2

Table 7: Results on mixed-numbers dataset

Results in Table 7 show that MoE models benefit from global inhibition gating. While dropout improves performance, it requires careful hyperparameter tuning. In contrast, adaptive inhibition methods automatically determine appropriate signal suppression levels, with performance scaling with connection diversity.

Algorithm	300K data	1M data
Baseline model	3.69e-6	1.17e-8
MoE 3/10 experts	3.68e-6	2.52e-10
PRE	3.37e-6	1.82e-10
CIGI/GRIN	**3.31e-6**	**1.81e-10**

Table 8: WMT English monolingual dataset (normalized log-likelihood loss)

5.3 LANGUAGE MODEL EXPERIMENT

We experiment with the transformer language model Vaswani et al. (2017); Shazeer et al. (2017); Du et al. (2022) with GRIN.

The MoE is applied on the fully connected layers of the transformer model, and gating heads is applied on the input of the MoE. The LM task is applied on WMT English monolingual dataset (Maillard et al., 2024) with one smaller set containing 300K sentences (7.5M words) and a larger one with 1 million sentences (25M words). Following the pre-processing, we train transformers. Table 8 shows test set normalized log-likelihood on next word prediction. The baseline MoE without gating performs similar to standard models, indicating less optimized routing and gating. Global inhibition yields visible improvements across both datasets, confirming its effectiveness for LM's.

6 Conclusion

We introduced the Global Recurrent Inhibition Network (GRIN), a novel architecture that enhances dynamic routing in Mixture of Experts models. GRIN implements a global inhibition head that recurrently processes diverse network activations and generate targeted gating signals. Our evaluation demonstrates improvements across tasks, particularly MTRL. For future work, we study the input spaces to GRIN with architecture specific designs and apply GRIN to more domains and in the multi-modal space. These directions enable learned optimization of gating strategies that surpass our current architectural design.

References

Rishabh Agarwal, Max Schwarzer, Pablo Samuel Castro, Aaron C Courville, and Marc Bellemare. Deep reinforcement learning at the edge of the statistical precipice. *Advances in neural information processing systems*, 34:29304–29320, 2021.

Jimmy Ba and Brendan Frey. Adaptive dropout for training deep neural networks. In C.J. Burges, L. Bottou, M. Welling, Z. Ghahramani, and K.Q. Weinberger (eds.), *Advances in Neural Information Processing Systems*, volume 26. Curran Associates, Inc., 2013. URL https://proceedings.neurips.cc/paper_files/paper/2013/file/7b5b23f4aadf9513306bcd59afb6e4c9-Paper.pdf.

Maxime Chevalier-Boisvert, Bolun Dai, Mark Towers, Rodrigo Perez-Vicente, Lucas Willems, Salem Lahlou, Suman Pal, Pablo Samuel Castro, and Jordan Terry. Minigrid & miniworld: Modular & customizable reinforcement learning environments for goal-oriented tasks. *Advances in Neural Information Processing Systems*, 36:73383–73394, 2023.

Marta Chini, Thomas Pfeffer, and Ileana Hanganu-Opatz. An increase of inhibition drives the developmental decorrelation of neural activity. *eLife*, 11:e78811, 2022. doi: 10.7554/eLife.78811. URL https://doi.org/10.7554/eLife.78811.

Yann N Dauphin, Angela Fan, Michael Auli, and David Grangier. Language modeling with gated convolutional networks. In *International conference on machine learning*, pp. 933–941. PMLR, 2017a.

Yann N. Dauphin, Angela Fan, Michael Auli, and David Grangier. Language modeling with gated convolutional networks, 2017b. URL https://arxiv.org/abs/1612.08083.

Carlo D'Eramo, Davide Tateo, Andrea Bonarini, Marcello Restelli, and Jan Peters. Sharing knowledge in multi-task deep reinforcement learning. *arXiv preprint arXiv:2401.09561*, 2024.

Coline Devin, Abhishek Gupta, Trevor Darrell, Pieter Abbeel, and Sergey Levine. Learning modular neural network policies for multi-task and multi-robot transfer. In *2017 IEEE international conference on robotics and automation (ICRA)*, pp. 2169–2176. IEEE, 2017.

Nan Du, Yanping Huang, Andrew M Dai, Simon Tong, Dmitry Lepikhin, Yuanzhong Xu, Maxim Krikun, Yanqi Zhou, Adams Wei Yu, Orhan Firat, et al. Glam: Efficient scaling of language models with mixture-of-experts. In *International conference on machine learning*, pp. 5547–5569. PMLR, 2022.

Golnaz Ghiasi, Tsung-Yi Lin, and Quoc V. Le. Dropblock: A regularization method for convolutional networks, 2018. URL https://arxiv.org/abs/1810.12890.

Albert Gidon and Idan Segev. Principles governing the operation of synaptic inhibition in dendrites. *Neuron*, 75(2):330–341, 2012.

Shixiang Gu, Ethan Holly, Timothy Lillicrap, and Sergey Levine. Deep reinforcement learning for robotic manipulation with asynchronous off-policy updates. In *2017 IEEE international conference on robotics and automation (ICRA)*, pp. 3389–3396. IEEE, 2017.

David Ha, Andrew Dai, and Quoc V Le. Hypernetworks. *arXiv preprint arXiv:1609.09106*, 2016.

Tuomas Haarnoja, Aurick Zhou, Pieter Abbeel, and Sergey Levine. Soft actor-critic: Off-policy maximum entropy deep reinforcement learning with a stochastic actor. In *International conference on machine learning*, pp. 1861–1870. Pmlr, 2018.

Tao Han, Huaixuan Shi, Xinyi Ding, Xi-Ao Ma, Huamao Gu, and Yili Fang. Mixture of experts based multi-task supervise learning from crowds. In *Proceedings of the AAAI Conference on Artificial Intelligence*, volume 39, pp. 14256–14264, 2025.

Ahmed Hendawy, Jan Peters, and Carlo D'Eramo. Multi-task reinforcement learning with mixture of orthogonal experts. *arXiv preprint arXiv:2311.11385*, 2023.

Geoffrey E Hinton, Alex Krizhevsky, and Sida D Wang. Transforming auto-encoders. In *International conference on artificial neural networks*, pp. 44–51. Springer, 2011.

Geoffrey E Hinton, Sara Sabour, and Nicholas Frosst. Matrix capsules with em routing. In *International conference on learning representations*, 2018.

Sepp Hochreiter and Jürgen Schmidhuber. Long short-term memory. *Neural computation*, 9(8): 1735–1780, 1997.

Sonja B Hofer, Ho Ko, Bruno Pichler, Joshua Vogelstein, Hana Ros, Hongkui Zeng, Ed Lein, Nicholas A Lesica, and Thomas D Mrsic-Flogel. Differential connectivity and response dynamics of excitatory and inhibitory neurons in visual cortex. *Nature neuroscience*, 14(8):1045–1052, 2011.

Jeffry S. Isaacson and Massimo Scanziani. How inhibition shapes cortical activity. *Neuron*, 72(2):231–243, 2011. ISSN 0896-6273. doi: https://doi.org/10.1016/j.neuron.2011.09.027. URL https://www.sciencedirect.com/science/article/pii/S0896627311008798.

Motoki Kajiwara, Ritsuki Nomura, Felix Goetze, Masanori Kawabata, Yoshikazu Isomura, Tatsuya Akutsu, and Masanori Shimono. Inhibitory neurons exhibit high controlling ability in the cortical microconnectome. *PLOS Computational Biology*, 17(4):e1008846, 2021.

Dmitry Kalashnikov, Alex Irpan, Peter Pastor, Julian Ibarz, Alexander Herzog, Eric Jang, Deirdre Quillen, Ethan Holly, Mrinal Kalakrishnan, Vincent Vanhoucke, et al. Scalable deep reinforcement learning for vision-based robotic manipulation. In *Conference on robot learning*, pp. 651–673. PMLR, 2018.

Diederik P. Kingma, Tim Salimans, and Max Welling. Variational dropout and the local reparameterization trick, 2015. URL https://arxiv.org/abs/1506.02557.

Thomas Klausberger and Peter Somogyi. Neuronal diversity and temporal dynamics: the unity of hippocampal circuit operations. *Science*, 321(5885):53–57, 2008.

Yilun Kong, Guozheng Ma, Qi Zhao, Haoyu Wang, Li Shen, Xueqian Wang, and Dacheng Tao. Mastering massive multi-task reinforcement learning via mixture-of-expert decision transformer. *arXiv preprint arXiv:2505.24378*, 2025.

Adam Kosiorek, Sara Sabour, Yee Whye Teh, and Geoffrey E Hinton. Stacked capsule autoencoders. *Advances in neural information processing systems*, 32, 2019.

Bonan Li, Yinhan Hu, Xuecheng Nie, Congying Han, Xiangjian Jiang, Tiande Guo, and Luoqi Liu. Dropkey, 2023. URL https://arxiv.org/abs/2208.02646.

Timothy P Lillicrap, Jonathan J Hunt, Alexander Pritzel, Nicolas Heess, Tom Erez, Yuval Tassa, David Silver, and Daan Wierstra. Continuous control with deep reinforcement learning. *arXiv preprint arXiv:1509.02971*, 2015.

Yue Liu, Christos Matsoukas, Fredrik Strand, Hossein Azizpour, and Kevin Smith. Patchdropout: Economizing vision transformers using patch dropout, 2022. URL https://arxiv.org/abs/2208.07220.

Jiaqi Ma, Zhe Zhao, Xinyang Yi, Jilin Chen, Lichan Hong, and Ed H Chi. Modeling task relationships in multi-task learning with multi-gate mixture-of-experts. In *Proceedings of the 24th ACM SIGKDD international conference on knowledge discovery & data mining*, pp. 1930–1939, 2018.

Jean Maillard, Laurie Burchell, Antonios Anastasopoulos, Christian Federmann, Philipp Koehn, and Skyler Wang. Findings of the WMT 2024 shared task of the open language data initiative. In Barry Haddow, Tom Kocmi, Philipp Koehn, and Christof Monz (eds.), *Proceedings of the Ninth Conference on Machine Translation*, pp. 110–117, Miami, Florida, USA, November 2024. Association for Computational Linguistics. doi: 10.18653/v1/2024.wmt-1.4. URL https://aclanthology.org/2024.wmt-1.4/.

Henry Markram, Maria Toledo-Rodriguez, Yun Wang, Anirudh Gupta, Gilad Silberberg, and Caizhi Wu. Interneurons of the neocortical inhibitory system. *Nature reviews neuroscience*, 5(10):793–807, 2004.

Volodymyr Mnih, Koray Kavukcuoglu, David Silver, Alex Graves, Ioannis Antonoglou, Daan Wierstra, and Martin Riedmiller. Playing atari with deep reinforcement learning. *arXiv preprint arXiv:1312.5602*, 2013.

Ethan Perez, Florian Strub, Harm De Vries, Vincent Dumoulin, and Aaron Courville. Film: Visual reasoning with a general conditioning layer. In *Proceedings of the AAAI conference on artificial intelligence*, volume 32, 2018.

Carsten K Pfeffer, Mingshan Xue, Miao He, Z Josh Huang, and Massimo Scanziani. Inhibition of inhibition in visual cortex: the logic of connections between molecularly distinct interneurons. *Nature neuroscience*, 16(8):1068–1076, 2013.

Hieu Pham, Melody Guan, Barret Zoph, Quoc Le, and Jeff Dean. Efficient neural architecture search via parameters sharing. In *International conference on machine learning*, pp. 4095–4104. PMLR, 2018.

Zihan Qiu, Zekun Wang, Bo Zheng, Zeyu Huang, Kaiyue Wen, Songlin Yang, Rui Men, Le Yu, Fei Huang, Suozhi Huang, et al. Gated attention for large language models: Non-linearity, sparsity, and attention-sink-free. *arXiv preprint arXiv:2505.06708*, 2025.

Jathushan Rajasegaran, Vinoj Jayasundara, Sandaru Jayasekara, Hirunima Jayasekara, Suranga Seneviratne, and Ranga Rodrigo. Deepcaps: Going deeper with capsule networks. In *Proceedings of the IEEE/CVF conference on computer vision and pattern recognition*, pp. 10725–10733, 2019.

Sara Sabour, Nicholas Frosst, and Geoffrey E Hinton. Dynamic routing between capsules. *Advances in neural information processing systems*, 30, 2017.

Noam Shazeer. Glu variants improve transformer, 2020. URL https://arxiv.org/abs/2002.05202.

Noam Shazeer, Azalia Mirhoseini, Krzysztof Maziarz, Andy Davis, Quoc Le, Geoffrey Hinton, and Jeff Dean. Outrageously large neural networks: The sparsely-gated mixture-of-experts layer, 2017. URL https://arxiv.org/abs/1701.06538.

Shagun Sodhani, Amy Zhang, and Joelle Pineau. Multi-task reinforcement learning with context-based representations. In *International conference on machine learning*, pp. 9767–9779. PMLR, 2021.

Rupesh Kumar Srivastava, Klaus Greff, and Jürgen Schmidhuber. Highway networks. *CoRR*, abs/1505.00387, 2015. URL http://arxiv.org/abs/1505.00387.

Kenneth O Stanley, David B D'Ambrosio, and Jason Gauci. A hypercube-based encoding for evolving large-scale neural networks. *Artificial life*, 15(2):185–212, 2009.

Ivilin Stoianov and Marco Zorzi. Emergence of a'visual number sense'in hierarchical generative models. *Nature neuroscience*, 15(2):194–196, 2012.

Lingfeng Sun, Haichao Zhang, Wei Xu, and Masayoshi Tomizuka. Paco: Parameter-compositional multi-task reinforcement learning. *Advances in Neural Information Processing Systems*, 35: 21495–21507, 2022.

Olivia K Swanson and Arianna Maffei. From hiring to firing: activation of inhibitory neurons and their recruitment in behavior. *Frontiers in molecular neuroscience*, 12:168, 2019.

Yee Teh, Victor Bapst, Wojciech M Czarnecki, John Quan, James Kirkpatrick, Raia Hadsell, Nicolas Heess, and Razvan Pascanu. Distral: Robust multitask reinforcement learning. *Advances in neural information processing systems*, 30, 2017.

Rémi Tremblay, Sophia Lee, and Bernardo Rudy. Gabaergic interneurons in the neocortex: from cellular properties to circuits. *Neuron*, 91(2):260–292, 2016.

Ashish Vaswani, Noam Shazeer, Niki Parmar, Jakob Uszkoreit, Llion Jones, Aidan N Gomez, Łukasz Kaiser, and Illia Polosukhin. Attention is all you need. *Advances in neural information processing systems*, 30, 2017.

Dilin Wang and Qiang Liu. An optimization view on dynamic routing between capsules. 2018.

Ruihan Yang, Huazhe Xu, Yi Wu, and Xiaolong Wang. Multi-task reinforcement learning with soft modularization. *Advances in Neural Information Processing Systems*, 33:4767–4777, 2020.

Tianhe Yu, Saurabh Kumar, Abhishek Gupta, Sergey Levine, Karol Hausman, and Chelsea Finn. Gradient surgery for multi-task learning. *Advances in neural information processing systems*, 33: 5824–5836, 2020a.

Tianhe Yu, Deirdre Quillen, Zhanpeng He, Ryan Julian, Karol Hausman, Chelsea Finn, and Sergey Levine. Meta-world: A benchmark and evaluation for multi-task and meta reinforcement learning. In *Conference on robot learning*, pp. 1094–1100. PMLR, 2020b.

Yiren Zhao, Oluwatomisin Dada, Xitong Gao, and Robert D Mullins. Revisiting structured dropout, 2022. URL https://arxiv.org/abs/2210.02570.

Barret Zoph and Quoc V Le. Neural architecture search with reinforcement learning. In *International Conference on Learning Representations*, 2017.

Barret Zoph, Vijay Vasudevan, Jonathon Shlens, and Quoc V Le. Learning transferable architectures for scalable image recognition. In *Proceedings of the IEEE conference on computer vision and pattern recognition*, pp. 8697–8710, 2018.

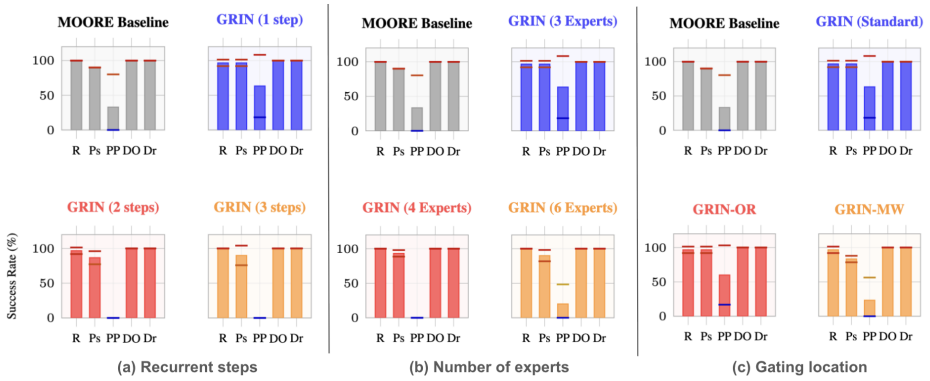

Figure 6: Ablation on MetaWorld MT5(a) Recurrent steps (b) Number of experts (c) Gating location. Task success rates (%) ± std bars for tasks R: Reach, Ps: Push, PP: Pick Place, DO: Door Open, Dr: Drawer

A Appendix

A.1 Extended Background and Literature Review

Extensions to dropout and dynamic architectures include adapting parameters through additional network models in Hypernetworks (Ha et al., 2016) and HyperNEAT (Stanley et al., 2009). Neural architecture search uses reinforcement learning to choose network architectures (Pham et al., 2018; Zoph & Le, 2017; Zoph et al., 2018).

Related to Capsules, (Wang & Liu, 2018) offers an optimization perspective, (Kosiorek et al., 2019) proposes autoencoders with capsules, and (Rajasegaran et al., 2019) builds a deeper network.

Related to MTRL, multi-task learning exists in other domains such as supervised learning (Han et al., 2025) and recommender systems (Ma et al., 2018).

A.2 MTRL GRIN Implementation Details

We implement GRIN in pytorch using two system generalizations. First, we leverage the forward hook registered in pytorch *nn.Module* that triggers automated storing of any activations $\mathbf{a}$ and their gradient computation graph. This enables the storage of activations in efficient hash data-structures. Second the pytorch module traversal is used to search global and diverse sets of inputs for the inhibition head. For efficiency, we cache the activations before l for the recurrent iterations, where l is the earliest point of dynamic modulation and gating. The caching can be done for cases where inputs are non-sequential and identical.

A.3 Ablation Bar Charts on MetaWorld MT5 (Figure. 7)

A.4 Mixed-numbers and Language Model Data and Implementation details

The data set is composed of 60,000 MNIST handwritten digits and 60,000 synthetic square number patterns following (Stoianov & Zorzi, 2012). The baseline architecture employs a two-layer convolutional network with max-pooling, augmented with a sparsely gated Mixture-of-Experts layer containing 5 experts (128-unit MLPs each). K=3 experts are selected per sample via a learned router. Results in Table 7 show that MoE models benefit from global inhibition gating for handling multi-modal inputs, models with more global inhibitory connections outperform those with local inhibition on this recognition task on multi-modal vision data.

Pre-processing details for the WMT dataset: we perform lower-casing, Porter stemming, digit replacement, contraction expansion, and punctuation removal. Transformer architecture: two-layers, embedding, hidden dimension is 50, 2 heads. We use vocabulary sizes of 8,500 and 15,000 for the

respective datasets (300k, 1m) and models are trained with Adam with a learning rate of 0.001 and batch size of 256. For each MoE we use 10 experts and each data points assigns K=3 experts.

A.5 Experiments and Ablation on Minigrid

Table 9: MiniGrid MT7 Results at Epoch 46: Average Return across 10 random seeds

Algorithm	4 Experts	6 Experts	8 Experts
MOORE	0.7501 ± 0.0604	**0.7746 ± 0.0606**	**0.7831 ± 0.0413**
GRIN	0.7530 ± 0.0545	0.7523 ± 0.0490	0.7449 ± 0.0761
GRIN light	**0.7759 ± 0.0612**	**0.7754 ± 0.0535**	0.7657 ± 0.0543

Table 10: MiniGrid MT7 Performance Comparison at Epoch 46

Experts	MOORE	GRIN	GRIN light
4	0.7501	0.7530	**0.7759**
6	0.7746	0.7523	**0.7754**
8	**0.7831**	0.7449	0.7657

Table 11: MiniGrid MT7 Detailed Results at Epoch 46

Experiment	Algorithm	Experts	Seeds	Average Return
GRIN with 4 experts	GRIN	4	10	0.7530 ± 0.0545
GRIN with 6 experts	GRIN	6	10	0.7523 ± 0.0490
GRIN with 8 experts	GRIN	8	10	0.7449 ± 0.0761
GRIN light with 4 experts	GRIN_light	4	10	0.7759 ± 0.0612
GRIN light with 6 experts	GRIN_light	6	10	0.7754 ± 0.0535
GRIN light with 8 experts	GRIN_light	8	10	0.7657 ± 0.0543
MOORE with 4 experts	MOORE	4	10	0.7501 ± 0.0604
MOORE with 6 experts	MOORE	6	10	0.7746 ± 0.0606
MOORE with 8 experts	MOORE	8	10	0.7831 ± 0.0413
MOORE Average	**MOORE**	**All**	-	**0.7693**
GRIN Average	**GRIN**	**All**	-	**0.7612**

A.6 Detailed Experiment Results

Table 12: MT50 Results Comparison at Epoch 4: MOORE Baseline (10 seeds) vs MOORE with GRIN (10 seeds)

Task	Success Rate		Mean J (reward)		Discounted Mean J	
	Baseline	GRIN	Baseline	GRIN	Baseline	GRIN
Overall Average	**0.4650 ± 0.4769**	**0.4848 ± 0.4764**	-	-	-	-
Assembly	0.0000 ± 0.0000	0.0000 ± 0.0000	231.23 ± 153.79	360.68 ± 185.50	109.23 ± 64.05	164.93 ± 77.42
Basketball	0.0000 ± 0.0000	0.0000 ± 0.0000	3.51 ± 0.74	5.40 ± 1.54	1.81 ± 0.36	2.69 ± 0.72
Bin Picking	0.0000 ± 0.0000	0.0000 ± 0.0000	3.88 ± 1.59	4.35 ± 1.60	1.98 ± 0.75	2.19 ± 0.74
Box Close	0.0000 ± 0.0000	0.0000 ± 0.0000	184.02 ± 21.20	195.41 ± 17.73	101.25 ± 10.36	106.43 ± 8.01
Button Press Topdown	0.8500 ± 0.3074	0.8600 ± 0.3007	794.87 ± 154.44	829.03 ± 116.02	323.64 ± 58.20	337.73 ± 42.97
Button Press Topdown Wall	0.7000 ± 0.4583	0.6600 ± 0.4363	728.81 ± 174.50	764.72 ± 122.01	298.81 ± 62.66	313.97 ± 45.32
Button Press	0.5400 ± 0.4055	0.6800 ± 0.4468	586.69 ± 267.03	666.91 ± 257.10	262.04 ± 112.79	295.88 ± 108.60
Button Press Wall	0.9500 ± 0.0671	0.8100 ± 0.3113	705.39 ± 143.22	703.72 ± 178.43	311.79 ± 59.57	308.64 ± 71.96
Coffee Button	0.9300 ± 0.1100	0.9700 ± 0.0900	856.20 ± 99.27	959.09 ± 80.96	392.75 ± 41.87	431.45 ± 35.74
Coffee Pull	0.0000 ± 0.0000	0.0000 ± 0.0000	7.30 ± 1.43	27.00 ± 51.27	3.74 ± 0.70	11.87 ± 20.81
Coffee Push	0.0000 ± 0.0000	0.1000 ± 0.3000	7.17 ± 0.98	77.27 ± 207.91	3.71 ± 0.42	29.56 ± 76.40
Dial Turn	0.7400 ± 0.1855	0.8600 ± 0.1114	802.69 ± 220.18	961.19 ± 103.92	358.42 ± 91.33	423.90 ± 47.50
Disassemble	0.0000 ± 0.0000	0.0000 ± 0.0000	59.09 ± 6.78	58.36 ± 1.64	31.18 ± 3.57	30.78 ± 0.87
Door Close	1.0000 ± 0.0000	1.0000 ± 0.0000	1029.50 ± 8.42	1025.88 ± 18.68	403.54 ± 5.19	401.60 ± 11.22
Door Lock	0.9800 ± 0.0600	0.9100 ± 0.1814	1000.94 ± 40.38	1009.83 ± 83.52	459.33 ± 22.30	467.73 ± 40.71
Door Open	0.3500 ± 0.4365	0.6700 ± 0.4428	631.00 ± 220.49	778.03 ± 189.37	272.43 ± 77.71	326.51 ± 64.03
Door Unlock	0.9800 ± 0.0600	0.9700 ± 0.0458	1163.95 ± 59.79	1180.55 ± 42.04	528.65 ± 28.07	537.89 ± 22.02
Drawer Close	1.0000 ± 0.0000	1.0000 ± 0.0000	1319.57 ± 71.68	1338.39 ± 28.96	625.54 ± 31.42	633.60 ± 12.69
Drawer Open	0.5800 ± 0.4750	0.8800 ± 0.2960	994.69 ± 192.38	1117.33 ± 112.02	467.22 ± 81.23	519.12 ± 47.54
Faucet Open	0.0000 ± 0.0000	0.0000 ± 0.0000	601.44 ± 8.63	610.43 ± 4.87	302.26 ± 4.04	306.25 ± 1.97
Faucet Close	0.8900 ± 0.2982	0.8900 ± 0.2982	1176.43 ± 189.00	1169.61 ± 204.14	537.53 ± 77.54	533.20 ± 83.86
Hammer	0.0900 ± 0.2119	0.1800 ± 0.3059	285.55 ± 211.38	507.40 ± 298.91	132.69 ± 86.29	225.14 ± 120.50
Hand Insert	0.2300 ± 0.2326	0.5300 ± 0.3926	162.31 ± 137.83	635.83 ± 367.14	64.69 ± 53.82	276.98 ± 160.43
Handle Press Side	1.0000 ± 0.0000	1.0000 ± 0.0000	1343.77 ± 12.74	1340.83 ± 5.25	634.97 ± 10.03	632.45 ± 4.03
Handle Press	1.0000 ± 0.0000	1.0000 ± 0.0000	1371.56 ± 15.18	1352.68 ± 27.42	659.50 ± 12.77	645.93 ± 17.97
Handle Pull Side	0.6000 ± 0.4899	0.4000 ± 0.4899	620.08 ± 506.85	404.53 ± 500.30	247.21 ± 203.04	167.70 ± 205.71
Handle Pull	0.3000 ± 0.4583	0.2300 ± 0.3951	660.42 ± 237.34	615.60 ± 213.67	295.31 ± 75.76	279.21 ± 70.74
Lever Pull	0.0000 ± 0.0000	0.0000 ± 0.0000	177.44 ± 6.72	174.44 ± 4.89	89.73 ± 2.79	88.60 ± 2.38
Peg Insert Side	0.0000 ± 0.0000	0.0000 ± 0.0000	4.61 ± 3.55	35.14 ± 92.28	2.24 ± 1.44	14.83 ± 38.07
Peg Unplug Side	0.0000 ± 0.0000	0.3100 ± 0.4346	5.24 ± 1.36	257.79 ± 387.04	2.77 ± 0.67	102.86 ± 153.54
Pick Place Wall	0.0000 ± 0.0000	0.0000 ± 0.0000	0.00 ± 0.00	0.00 ± 0.00	0.00 ± 0.00	0.00 ± 0.00
Pick Out Of Hole	0.0000 ± 0.0000	0.0000 ± 0.0000	2.68 ± 0.43	2.86 ± 0.22	1.38 ± 0.22	1.48 ± 0.11
Pick Place	0.0000 ± 0.0000	0.0000 ± 0.0000	2.47 ± 0.78	3.65 ± 0.86	1.28 ± 0.39	1.89 ± 0.43
Plate Slide	0.9800 ± 0.0400	0.9300 ± 0.1418	1075.83 ± 83.20	1044.71 ± 83.52	455.12 ± 38.62	445.87 ± 32.55
Plate Slide Side	0.9200 ± 0.1470	0.9100 ± 0.1814	914.24 ± 132.92	1009.38 ± 128.67	422.18 ± 53.74	457.21 ± 40.24
Plate Slide Back	0.9900 ± 0.0300	1.0000 ± 0.0000	1240.71 ± 47.59	1258.33 ± 50.87	562.90 ± 28.33	574.76 ± 22.92
Plate Slide Back Side	1.0000 ± 0.0000	0.8100 ± 0.2809	1252.73 ± 14.69	1127.90 ± 222.28	567.86 ± 9.06	510.63 ± 97.01
Push Back	0.0100 ± 0.0300	0.0100 ± 0.0300	7.88 ± 2.29	11.29 ± 6.97	3.79 ± 1.10	5.29 ± 3.00
Push	0.2450 ± 0.2307	0.1850 ± 0.2098	299.74 ± 244.55	329.69 ± 212.78	133.77 ± 108.93	150.47 ± 95.01
Push Wall	0.0100 ± 0.0300	0.0000 ± 0.0000	185.91 ± 266.21	363.38 ± 258.71	85.37 ± 116.02	168.76 ± 115.87
Reach	0.9400 ± 0.0663	0.9600 ± 0.0490	1342.59 ± 12.75	1346.45 ± 7.40	641.34 ± 7.54	642.01 ± 4.92
Reach Wall	0.9700 ± 0.0458	0.9600 ± 0.1200	1318.39 ± 14.23	1315.76 ± 30.08	622.43 ± 5.93	621.07 ± 14.27
Shelf Place	0.0000 ± 0.0000	0.0000 ± 0.0000	0.01 ± 0.03	0.06 ± 0.16	0.01 ± 0.02	0.03 ± 0.07
Soccer	0.4300 ± 0.3848	0.4600 ± 0.3262	427.37 ± 363.84	419.29 ± 252.71	180.68 ± 153.76	180.90 ± 105.18
Stick Pull	0.0000 ± 0.0000	0.0000 ± 0.0000	4.75 ± 1.59	5.31 ± 0.83	2.46 ± 0.75	2.75 ± 0.40
Sweep Into	0.5800 ± 0.4771	0.7300 ± 0.4051	785.79 ± 387.01	1001.91 ± 305.98	358.69 ± 169.19	457.60 ± 134.81
Sweep	0.0000 ± 0.0000	0.0000 ± 0.0000	168.00 ± 72.12	256.93 ± 171.44	79.93 ± 33.35	117.49 ± 68.80
Window Open	1.0000 ± 0.0000	0.9900 ± 0.0300	1016.99 ± 41.21	1022.67 ± 50.52	410.08 ± 20.59	411.92 ± 24.61
Window Close	1.0000 ± 0.0000	0.9000 ± 0.3000	1045.53 ± 79.82	929.26 ± 269.54	427.96 ± 40.67	379.61 ± 106.33

Table 13: MT3 Results (3 Tasks) - Mean ± Std across 5 seeds

Experiment	Task	Success Rate	Mean J (Reward)	Discounted Mean J
MT3 Baseline (256hd, 2 layers)	Reach-v2	1.000 ± 0.000	1336.18 ± 16.97	631.05 ± 13.89
	Push-v2	0.100 ± 0.200	45.86 ± 60.89	26.69 ± 35.61
	Pick-Place-v2	0.000 ± 0.000	**2.15 ± 1.43**	**1.17 ± 0.74**
MT3 Pretext Inhi. (weights only, 256hd, 2 layers)	Reach-v2	**1.000 ± 0.000**	**1346.20 ± 14.14**	**642.27 ± 10.18**
	Push-v2	**0.100 ± 0.200**	**62.23 ± 55.93**	**29.98 ± 23.95**
	Pick-Place-v2	0.000 ± 0.000	1.67 ± 0.36	0.96 ± 0.19

Table 14: MT5 Results (5 Tasks) - Mean ± Std across 5 seeds

Experiment	Task	Success Rate	Mean J (Reward)	Discounted Mean J
MT5 Baseline (256hd, 2 layers)	Reach-v2	1.000 ± 0.000	1350.54 ± 15.72	644.56 ± 12.72
	Push-v2	0.000 ± 0.000	33.10 ± 25.92	20.36 ± 16.97
	Pick-Place-v2	0.000 ± 0.000	1.85 ± 0.44	1.06 ± 0.28
	Door-Open-v2	0.000 ± 0.000	458.59 ± 44.02	215.29 ± 21.55
	Drawer-Open-v2	0.000 ± 0.000	**738.09 ± 25.11**	**358.31 ± 9.54**
MT5 Pretext Inhibition (weights + features, 256hd, 2 layers)	Reach-v2	1.000 ± 0.000	1340.13 ± 15.30	636.03 ± 11.92
	Push-v2	0.000 ± 0.000	17.82 ± 17.18	8.86 ± 7.57
	Pick-Place-v2	0.000 ± 0.000	1.46 ± 0.49	0.87 ± 0.28
	Door-Open-v2	0.000 ± 0.000	439.82 ± 120.14	203.16 ± 47.28
	Drawer-Open-v2	0.000 ± 0.000	675.73 ± 110.36	331.72 ± 48.61
MT5 Pretext Inhibition (weights only, 256hd, 2 layers)	Reach-v2	**1.000 ± 0.000**	**1351.29 ± 16.27**	**648.46 ± 7.86**
	Push-v2	0.000 ± 0.000	10.97 ± 8.08	6.31 ± 5.08
	Pick-Place-v2	0.000 ± 0.000	1.68 ± 0.38	0.94 ± 0.33
	Door-Open-v2	0.000 ± 0.000	457.90 ± 85.74	213.64 ± 34.67
	Drawer-Open-v2	0.000 ± 0.000	716.92 ± 30.14	349.03 ± 14.12
MT5 GRIN (rec=1) (weights + features, 256hd, 2 layers)	Reach-v2	1.000 ± 0.000	1311.13 ± 50.76	624.66 ± 19.35
	Push-v2	0.000 ± 0.000	**43.07 ± 18.62**	**21.90 ± 10.27**
	Pick-Place-v2	0.000 ± 0.000	2.02 ± 1.07	1.18 ± 0.59
	Door-Open-v2	0.000 ± 0.000	459.95 ± 33.94	217.50 ± 12.51
	Drawer-Open-v2	0.000 ± 0.000	718.56 ± 21.37	350.56 ± 8.39
MT5 GRIN (rec=3) (weights + features, 256hd, 2 layers)	Reach-v2	0.900 ± 0.200	1306.11 ± 72.21	627.65 ± 28.29
	Push-v2	0.000 ± 0.000	36.23 ± 22.20	18.57 ± 10.37
	Pick-Place-v2	0.000 ± 0.000	**2.37 ± 1.56**	**1.26 ± 0.80**
	Door-Open-v2	0.000 ± 0.000	409.93 ± 91.58	195.16 ± 40.73
	Drawer-Open-v2	0.000 ± 0.000	733.90 ± 48.66	356.60 ± 23.27
MT5 GRIN (rec=1) (weights only, 256hd, 2 layers)	Reach-v2	0.900 ± 0.200	1313.09 ± 58.16	626.27 ± 24.21
	Push-v2	0.000 ± 0.000	26.70 ± 7.30	15.13 ± 3.82
	Pick-Place-v2	0.000 ± 0.000	1.95 ± 0.59	1.06 ± 0.23
	Door-Open-v2	0.000 ± 0.000	**461.62 ± 17.06**	**217.69 ± 7.55**
	Drawer-Open-v2	0.000 ± 0.000	722.52 ± 17.35	351.05 ± 9.82

Table 15: MT10 Results Comparison at Epoch 20: MOORE Baseline (9 seeds) vs MOORE with GRIN (10 seeds)

Task	Success Rate		Mean J		Discounted Mean J	
	Baseline	GRIN	Baseline	GRIN	Baseline	GRIN
Overall Average	**0.8844 ± 0.3137**	**0.8820 ± 0.3135**	-	-	-	-
Reach	0.9778 ± 0.0629	0.9700 ± 0.0900	1350.86 ± 9.58	1351.25 ± 12.89	643.48 ± 7.06	645.07 ± 9.72
Push	1.0000 ± 0.0000	0.9500 ± 0.1025	1165.10 ± 92.92	1180.19 ± 94.50	507.36 ± 61.12	526.68 ± 53.01
Pick Place	0.0000 ± 0.0000	0.0000 ± 0.0000	2.78 ± 0.84	4.83 ± 2.01	1.42 ± 0.43	2.45 ± 0.92
Door Open	1.0000 ± 0.0000	1.0000 ± 0.0000	1067.50 ± 21.55	1043.79 ± 45.21	445.38 ± 12.66	432.47 ± 21.60
Drawer Open	0.8778 ± 0.3119	1.0000 ± 0.0000	1203.17 ± 165.46	1266.55 ± 22.76	562.34 ± 71.38	587.66 ± 11.94
Drawer Close	1.0000 ± 0.0000	1.0000 ± 0.0000	1359.86 ± 4.67	1354.25 ± 4.49	647.33 ± 4.10	642.47 ± 3.87
Button Press Topdown	1.0000 ± 0.0000	1.0000 ± 0.0000	906.88 ± 14.24	880.70 ± 25.45	372.22 ± 7.41	358.76 ± 12.05
Peg Insert Side	0.9889 ± 0.0314	0.9000 ± 0.3000	1096.05 ± 30.69	1037.75 ± 144.47	453.41 ± 13.36	423.62 ± 59.19
Window Open	1.0000 ± 0.0000	1.0000 ± 0.0000	1083.37 ± 17.57	1078.88 ± 22.52	443.51 ± 11.29	446.55 ± 13.32
Window Close	1.0000 ± 0.0000	1.0000 ± 0.0000	1063.78 ± 45.47	1082.34 ± 21.52	435.26 ± 23.63	444.50 ± 13.98